JOURNAL OF MATERIALS SCIENCE **34** (1999) 1595–1609

Influence of pore geometry on the effective response of porous media

C. T. HERAKOVICH, S. C. BAXTER*
University of Virginia, Charlottesville, VA 22903-2442, USA
E-mail: herak@virginia.edu

The generalized method of cells (GMC) is used to study the influence of pore geometry on the effective elastic properties and inelastic response of porous materials. Periodic microstructures with four distinct pore geometries are studied and the results for effective elastic properties are compared with several other available models and experimental results. Predictions for the inelastic response of porous alumina are presented for tensile loading, as a function of pore geometry and pore volume fraction, with the inelastic behavior of the bulk material modeled using a unified visco-plasticity theory. All results are presented for discrete pore shape and discrete porosity. It is shown that pore geometry can have a significant influence on both elastic and inelastic response, that pore geometry can be associated with parameters from other models, and that the generalized method of cells is an efficient, flexible and reliable method of analysis for such problems. © *1999 Kluwer Academic Publishers*

1. Introduction

The subject of porosity has received renewed attention in recent years. This is true for ceramics, metals and composites. Reasons for studying porosity include the fact that materials are often porous as the result of processing, that naturally occurring materials such as wood and bone are porous, and that advantageous engineering properties may be realized by taking advantage of porosity. Possible advantageous properties might include specific stiffness and strength, improved thermal conductivity, and resistance to crack growth. Materials may be porous because the fabrication process results in pores between particles that were not fully consolidated or they may be porous by design in order to affect a specific property. Materials that are porous by design are often referred to as cellular solids. Porous media typically have lower percent porosity than cellular solids. For all materials, it is desired to know the mechanical and physical properties as a function of the type(s) of porosity (pore geometry) and the degree of porosity expressed as a volume fraction or as relative density, i.e., the ratio of the density of the porous media to that of the nonporous solid. The focus of the present paper is directed toward porous media; the methods of analysis, however, would also be appropriate for cellular solids.

Recent review articles on porous media include those by Rice [1, 2]. Cellular solids are reviewed in the book by Gibson and Ashby [3]. It is interesting to note that there have been two fundamental approaches to the study of porous media. These approaches can be divided into those of the mechanics community and those of the materials community. The mechanics community has tended to consider a specific shape pore (most often spherical) and then develop analytical solutions for the properties as a function of the pore volume fraction. In contrast, the materials community has tended to obtain experimental results for the properties as a function of porosity and then found the "best fit" curve where the parameters are associated with the pore geometry or method of fabrication. It is also interesting that a review of the papers in the mechanics literature and those in the materials literature indicates that the interaction between the two communities is somewhat limited.

The majority of mechanics papers directed toward mechanical properties of porous media are concerned with elastic properties (e.g., Budiansky [4], MacKenzie [5], Nemat-Nasser and Taya [6]). Previous studies on inelastic response are those by Chu and Hashin [7] who used the composite spheres model to study the response of porous steel under dilatational loading. Carroll and Holt [8] and Butcher *et al.* [9] considered compressibility and dynamics effects, and Aboudi [10] used the original method of cells to study inelastic normal, dilatational and shear response of porous, elastic perfectly-plastic and elastoplastic work-hardening solids. All of the above papers are concerned with spherical pores (or approximations to spherical pores in the case of the method of cells).

The goal of the present work is to assess the applicability of the generalized method of cells (GMC) (Paley & Aboudi [11], Aboudi [12]) for calculating the effective elastic properties and inelastic response of a porous material as a function of pore geometry and percent porosity. The four pore shapes selected for consideration are: cylinder, cube, sphere and cross. Comparisons will be made with previously published experimental

* Now with the University of South Carolina, Columbia, SC.

data as well as with several other theoretical models. For the purpose of comparison, GMC is used to predict the effective behavior of aluminum oxide, Al_2O_3, a porous ceramic whose effective elastic behavior is well documented in the literature, and a glass that was die-pressed and sintered from a glass powder or frit. Predictions for nonlinear response are presented for the intermetallic compound IC-50 (Ni_3Al), a nickel aluminide (Ni-Al 23., Hf.5, B.2) at %.

All results presented in this paper are for periodic structures with discrete pore shape, stacking arrangement and porosity, and it is assumed that these parameters do not change during loading. However, it is important to note that the methodology presented has much broader capabilities. It is possible to model any shape pore that can be described in the cartesian geometry of the unit cell. Different stacking arrangements and combinations of pore shapes can be modeled as long as the microstructure is periodic at some level or a statistical approach is employed. In addition, the model can be extended to changing pore structure (shape and stacking arrangement) as a function of load history through the incorporation of finite deformation effects.

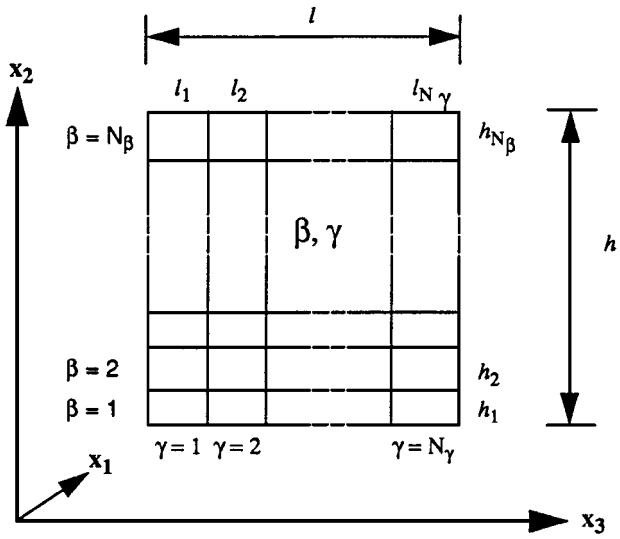

Figure 1 GMC representative repeating unit cell for 2-D.

2. The generalized method of cells

The generalized method of cells (GMC) is a computationally efficient and robust micromechanics analysis method for heterogeneous materials including porous media and composites. Thermal, mechanical (stress or strain control) and thermo-mechanical load histories can be imposed and a variety of constitutive laws for elastic and/or inelastic response of the constituents may be utilized. The constitutive model used for inelastic response in the present study is the Bodner and Partom [13] viscoplastic model. GMC is an extension of the original method of cells (Aboudi, [14]) which was used previously to study the inelastic response of porous media for one specific pore geometry (Aboudi [10]). Since the CTE of a porous, but otherwise homogeneous, medium is not influenced by porosity, thermal effects are not considered in this paper.

GMC considers a material that possesses a periodic structure such that a repeating, representative volume element can be identified in the form of a unit cell. A two-dimensional representative unit cell is shown in Fig. 1 and the three-dimensional unit cells to describe each of the four pore geometries considered in this paper, cylinder, cube, cross and sphere, and shown in Figs 2 to 5.

The 2-D representative repeating cell consists of $N_\beta \times N_\gamma$ subcells whereas the 3-D representation consists of $N_\alpha \times N_\beta \times N_\gamma$ subcells. Each one of these subcells can be occupied in general by any viscoplastic material. The constitutive law of such a material can be written in the form

$$\sigma = C(\varepsilon - \varepsilon^I) \tag{1}$$

where σ is the stress vector, and $\varepsilon, \varepsilon^I$ are the total and inelastic strains, respectively, and C is the elastic stiffness matrix of the material. The subcells corresponding to pores were represented as a linearly elastic material with very small Young's modulus, E, and relatively large Poisson's ratio, ν, resulting in a very small shear modulus through the isotropic relationship $G = E/2(1 + \nu)$.

The constitutive law was represented as a relationship between the rates of the field variables for use with the

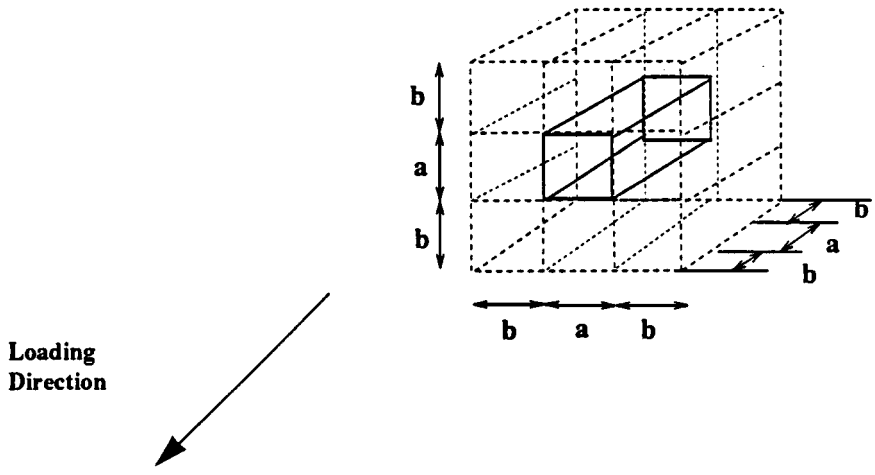

Figure 2 Cylindrical pore.

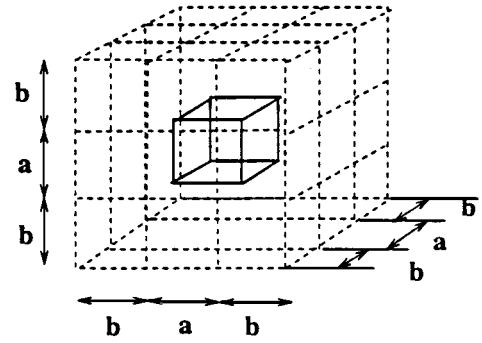

Figure 3 Cubic pore.

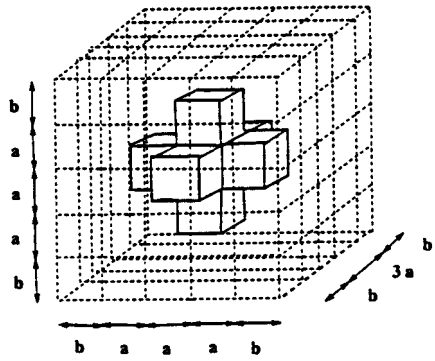

Figure 4 Cross shaped pore.

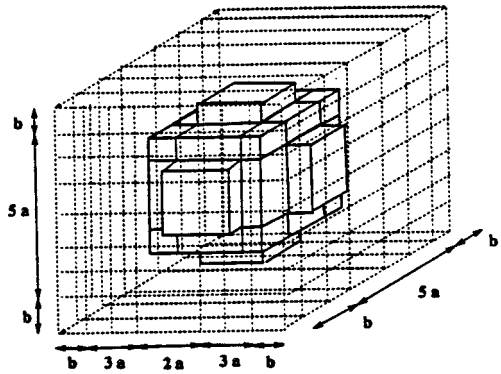

Figure 5 Spherical pore.

viscoplastic model. This tangent formulation can be established by multiplying and dividing the inelastic terms in (1) by the scalar $s\dot{\varepsilon}$ where s is the deviatoric part of σ. The resulting constitutive law is

$$\dot{\sigma} = C^{\mathrm{VP}}\dot{\varepsilon} \tag{2}$$

where C^{VP} denotes the instantaneous stiffness tensor of the viscoplastic phase. It is given by:

$$C^{\mathrm{VP}}_{ijkl} = C_{ijkl} - \frac{C_{ijab}\dot{\varepsilon}^I_{ab}s_{kl}}{s_{rt}\dot{\varepsilon}_{rt}} \tag{3}$$

In the special case of an isotropic, viscoplastic material, the term $C_{ijkl}\dot{\varepsilon}^I_{kl}$ can be written in terms of a flow rule function, Λ, in the form:

$$C_{ijkl}\dot{\varepsilon}^I_{kl} = C_{ijkl}\Lambda s_{kl} = 2\mu\Lambda s_{ij} \tag{4}$$

Using (4), (3) can be written:

$$C^{\mathrm{VP}}_{ijkl} = \lambda\delta_{ij}\delta_{kl} + \mu(\delta_{ik}\delta_{jl} + \delta_{il}\delta_{jk}) - 2\mu\frac{s_{mn}\dot{\varepsilon}^I_{mn}}{s_{rt}\dot{\varepsilon}_{rt}}\frac{s_{ij}s_{kl}}{s_{pq}s_{pq}} \tag{5}$$

where λ and μ are the Lamé elastic constants, and δ_{ij} is the Kronecker delta.

The basic micromechanical GMC analysis consists of four steps as follows:

1. *Identification of the repeating unit cell.*

2. *Definition of the macroscopic average stresses $\bar{\sigma}$ and strain $\bar{\varepsilon}$ from the corresponding microscopic quantities (homogenization).* Referring to Fig. 1 (for the 2-D case), we have:

$$\bar{\sigma} = \frac{1}{hl}\sum_{\beta=1}^{N_\beta}\sum_{\gamma=1}^{N_\gamma} h_\beta l_\gamma \bar{\sigma}^{(\beta\gamma)} \tag{6}$$

$$\bar{\varepsilon} = \frac{1}{hl}\sum_{\beta=1}^{N_\beta}\sum_{\gamma=1}^{N_\gamma} h_\beta l_\gamma \bar{\varepsilon}^{(\beta\gamma)} \tag{7}$$

where $\bar{\sigma}^{(\beta\gamma)}$ and $\bar{\varepsilon}^{(\beta\gamma)}$ are the average stress and strain in the subcell $(\beta\gamma)$.

3. *Imposition of continuity of displacements and tractions at the interfaces between the subcells, as well as between the repeating cells.* These continuity conditions establish, in conjunction with equilibrium within each subcell, the relationships between the microscopic total and inelastic strains with the macroscopic strains via the mechanical and inelastic concentration tensors (localization). It can be shown (Paley and Aboudi [11]) that the strains in the subcells are given in terms of the macroscopic strains and the subcells inelastic strains in the form:

$$\bar{\varepsilon}^{(\beta\gamma)} = A^{(\beta\gamma)}\bar{\varepsilon} + D^{(\beta\gamma)}\varepsilon^I_s \tag{8}$$

where $A^{(\beta\gamma)}$ and $D^{(\beta\gamma)}$ are the appropriate concentration tensors, and ε^I, are the inelastic strains in all subcells.

4. *Derivation of the resulting overall (macroscopic) constitutive equation of the multi-phase media.* The resulting inelastic constitutive law is given by:

$$\bar{\sigma} = B^*(\bar{\varepsilon} - \bar{\varepsilon}^I) \tag{9}$$

In this constitutive equation B^* is the effective elastic stiffness tensor of the material which is given in a closed-form manner.

$$B^* = \frac{1}{hl}\sum_{\beta=1}^{N_\beta}\sum_{\gamma=1}^{N_\gamma} h_\beta l_\gamma C^{(\beta\gamma)}A^{(\beta\gamma)} \tag{10}$$

The inelastic strain tensor has the form:

$$\bar{\varepsilon}^I = \frac{-B^{*-1}}{hl}\sum_{\beta=1}^{N_\beta}\sum_{\gamma=1}^{N_\gamma} h_\beta l_\gamma C^{(\beta\gamma)}\left(D^{(\beta\gamma)}\varepsilon^I_s - \bar{\varepsilon}^{I(\beta\gamma)}\right) \tag{11}$$

Once the strain concentration tensors, mechanical $A^{(\beta\gamma)}$ and the inelastic $D^{(\beta\gamma)}$, have been determined, it is possible to establish the microscopic stress in the subcell in the form:

$$\bar{\sigma}^{(\beta\gamma)} = C^{(\beta\gamma)}\left[A^{(\beta\gamma)}\bar{\varepsilon} + D^{(\beta\gamma)}\varepsilon_s^I - \bar{\varepsilon}^{I(\beta\gamma)}\right] \quad (12)$$

For elastic response, the stresses are:

$$\bar{\sigma}^{(\beta\gamma)} = Q^{(\beta\gamma)}\bar{\sigma} \quad (13)$$

where $Q^{(\beta\gamma)}$ is the mechanical stress concentration tensor given by

$$Q^{(\beta\gamma)} = C^{(\beta\gamma)}A^{(\beta\gamma)}B^{*-1} \quad (14)$$

It is also possible to establish the instantaneous constitutive law that governs the overall inelastic response by employing the corresponding instantaneous laws of the constituents given by (2) directly in GMC. Alternatively, one can multiply and divide the inelastic terms in the rate form of (9) by the scalar $\bar{s}\dot{\bar{\varepsilon}}$ where $\bar{s}$ is the deviatoric part of $\bar{\sigma}$. This readily provides the following relation between the rates of the total and inelastic strains via the overall instantaneous stiffness tensor.

$$\dot{\bar{\sigma}} = B^{*\mathrm{VP}}\dot{\bar{\varepsilon}} \quad (15)$$

where

$$B^{*\mathrm{VP}}_{ijkl} = B^*_{ijkl} - \frac{B^*_{ijab}\dot{\bar{\varepsilon}}^I_{ab}\bar{s}_{kl}}{\bar{s}_{rt}\dot{\bar{\varepsilon}}_{rt}} \quad (16)$$

The constitutive law (9) can be employed to predict the nonlinear behavior of porous media from the knowledge of the material properties of the medium and taking the pore to have near zero stiffness.

3. Pore geometry

Since GMC includes a description of the micro-geometry of a subvolume of the material, it is possible to describe various pore shapes in some detail. There were two objectives in the selection and design of pore shape. First, the proportions of each shape had to remain constant even as the porosity changed. This provided a definition of each shape, independent of the porosity, and made it is possible to examine how changes in the shape of the pore alone affected the properties of the porous material. The second objective was to maintain the physical sense of the pore, keeping in mind that there is a limiting value of porosity for each pore shape, i.e., when the outer edge of a pore is extended to the sides of the unit cell. This can be seen in the case of perfectly spherical pores in a square packing arrangement. In the limiting case, the matrix material would fill the cusp shaped areas between the spherical pores. At this porosity, the spheres would touch each other at one point on each face of the unit cell, and the pores would be considered a continuous phase. Beyond this porosity, the spherical shape of the pore would be lost as neighboring pores merge. Mathematically, the maximum pore volume fraction which can be achieved by *spherical pores*, maintaining the pore shape, is 0.5236. Similarly, the maximum volume of a cusp shaped pore in the unit cell, which results from the stacking of *spherical particles*, the reverse of spherical pores, is 0.4764.

The three dimensional version of the generalized methods of cells uses rectangular subcells to describe each pore shape (see Figs 2 to 5), but since it calculates average values across the pore boundaries, the corners in the subcells do not produce stress concentrations or singularities. This means that GMC may not 'see' a cube when the pore is drawn as a cube; however it does distinguish between shapes based on relative dimensions. General characteristics of real pore shapes were included when possible in the GMC descriptions. For example, a cubic pore could physically extend through the entire range of porosity, and in the case of our spherical pore, a "cubical" approximation to a sphere was constructed which reached its maximum volume at 0.5236. (which is the maximum for a sphere in a cube). The cross shaped pore, which might approximate a cusped shaped pore, does not match the corresponding maximum volume for the pores which result from packing spherical particles. More complicated designs are required to produce a symmetric shape which has its maximum pore volume fraction of 0.4764. It is not clear which shape, in a rectangular geometry, would best approximate a cusp shaped pore. (See Qian *et al.* [15], for a discussion of variations in cusp shapes.) The cross shaped pore is used because of its simple geometric shape and because it has a maximum porosity between that of the cubic and spherical pores, which makes it useful in comparison. Thus, these pore shapes are intended to span a range of shapes, but not specifically model their namesakes.

The cylindrical pore is not a pore in the usual sense, but rather a long cylindrical void. The three remaining pores are traditional inclusions. The three shapes, labeled cube, cross and sphere, are used to approximate various void shapes which occur either naturally, as a result of incomplete consolidation during processing, or intentionally, in a process designed to produce a porous material. The regular distribution of pores throughout the matrix material approximates a material that is statistically homogeneous and effectively isotropic. The four pore shapes as modeled in GMC are described in the following.

3.1. Cylindrical pore

The cylindrical pore, with a square cross section (Fig. 2), is used to approximate the voids which occur during the consolidation of a layered material. The main axis of the cylinder is aligned in the loading direction, and the pores are arranged in a square stacking sequence. The resulting material is effectively transversely isotropic. This pore is described in GMC by a unit cell divided into 9 subcells. Each subcell runs the depth of the unit cell. The subcell that lies along the main axis of the cylinder is the void. The remaining subcells are of the non-porous material.

In this case, the pore volume fraction can be calculated by the relative area of the pore across the face of the unit cube. This area of the unit cell is normal-

ized to one, and the pore volume (area) fraction can be expressed as

$$P_{\text{cyl}} = a^2 \tag{17}$$

where a is the dimension of the square cross-sectional area. This pore can increase in size to fill the unit cube exactly so the pore volume fraction can range from $0 \leq P_{\text{cyl}} \leq 1$.

$P = 1$ is, of course, a degenerate case.

3.2. Cubic pore

The GMC unit cell for the cubic pore (Fig. 3) is divided into 27 subcells, $3 \times 3 \times 3$. The center subcell (the pore) is a cube, with dimensions, $a \times a \times a$. The dimension a will be referred to as the characteristic dimension.

The volume of the unit cell is normalized to one, so that the porosity, P_{cube}, is given by

$$P_{\text{cube}} = a^3 \tag{18}$$

The second length is defined as $b = (1 - a)/2$. In the limiting case where $b \to 0$, and $(a \to 1)$, thus

$$0 \leq P_{\text{cube}} \leq 1 \tag{19}$$

$P = 1$ is the degenerate case.

3.3. Cross pore

This pore is modeled by a unit cell divided into 125 subcells, $5 \times 5 \times 5$. The center layer of subcells models the pore as a cross with equal lengths for each of the legs and the center (Fig. 4). The pore is symmetric about all three axis, forming a three dimensional cross, or cruciform shape. The unit cell is again normalized to unit volume, thus the porosity is given by

$$P_{\text{cross}} = 7a^3 \tag{20}$$

The second length is given by $b = (1 - 3a)/2$. In the limiting case where $b \to 0$, $(a \to 1/3)$, the porosity is within the range

$$0 \leq P_{\text{cross}} \leq 0.295 \tag{21}$$

Equality holds on the right-hand side of (21) when the pores from adjacent unit cells are in contact.

3.4. Spherical pore

This pore (Fig. 5) is modeled by a unit cell divided into 343 subcells, $7 \times 7 \times 7$. Again a characteristic dimension a is used to define the pore dimensions and proportions. The resulting pore volume fraction is

$$P_{\text{sph}} = 65.45a^3 \tag{22}$$

With the unit cell normalized to volume = 1, the second length is $b = (1 - 5a)/2$, and for this pore shape, in the limit as $b \to 0$, $(a \to 1/5)$ and thus

$$0 \leq P_{\text{sph}} \leq 0.5236 \tag{23}$$

Again, equality on the right-hand side of (23) holds when pores from adjacent unit cells are in contact.

4. Results and discussion

4.1. Comparison with experimental results

Comparison with experimental data previously presented in the literature is invariably limited by the type of tests conducted and the assumptions made in evaluating the data acquired. Beam deflection, tension, torsion, hydrostatic loading, resonant frequency and wave propagation methods have all been used. Data have been acquired as deflections, strain gage measurements, light reflection and ultrasonic velocities. Invariably it is assumed that the porous material is homogeneous and isotropic for the purpose of extracting material property values from the theory associated with each type of test. The following comparisons are made with these caveats noted.

The effective elastic properties were predicted for porous alumina (Al_2O_3) using the bulk properties: $E = 386$ GPa, $G = 163$ GPa, and $\nu = 0.19$ as input to GMC. Results for the effective Young's modulus, E, effective Poisson's ratio, ν, and effective shear modulus, G, for cylindrical, cubic, spherical and cross pores are presented as a function of porosity, P, in Figs 6–8. The Young's modulus results (Fig. 6) and the shear modulus results (Fig. 8) include comparison with the experimental data of Coble and Kingery [16] who measured Young's modulus using transverse bending tests and shear modulus using torsion tests. Beam deflections were measured in the bending tests and strains were measured in the torsion tests utilizing a light source reflected from sapphire mirrors mounted on the sample.

Coble and Kingery also presented data for Poisson's ratio, but their values were based upon *average* data and, as a result, the Poisson's ratio for zero porosity ($\nu = 0.27$) was 50% higher than the value for isotropic response ($\nu = 0.18$). Because of this the reported experimental data are not presented in Fig. 7. Coble and Kingery did report a 50% decrease in Poisson's ratio as porosity increases from 0.0 to 0.5.

For the theoretical predictions, the Young's modulus and Poisson's ratio were predicted directly from GMC and the shear modulus was obtained using these values and the isotropic relationship $G = E/2(1 + \nu)$. In all cases, results are presented only for porosities in the range possible for each particular pore shape as dictated by the GMC approximation. When applying GMC to porous materials it is necessary to assign material properties to the pore. For all results presented in this paper the pore properties were taken to be: $E = 0.001$ MPa, $G = 0.0004$ MPa and $\nu = 0.25$. These values insured that the elastic stiffness C_{ij} are very small for the pore.

It is evident from the figures that an increase in porosity results in a degradation in all three elastic properties, with one exception, Poisson's ratio for cylindrical pores (Fig. 7). The results clearly are also a function of pore geometry. The cylindrical pore predictions give the smallest degradation of property and the predictions based upon the cross pore shape result in the largest degradation. The cubic and spherical pore predictions are intermediate, with the spherical pore always exhibiting more degradation than the cubic pore. There are significant differences in the predictions (more than

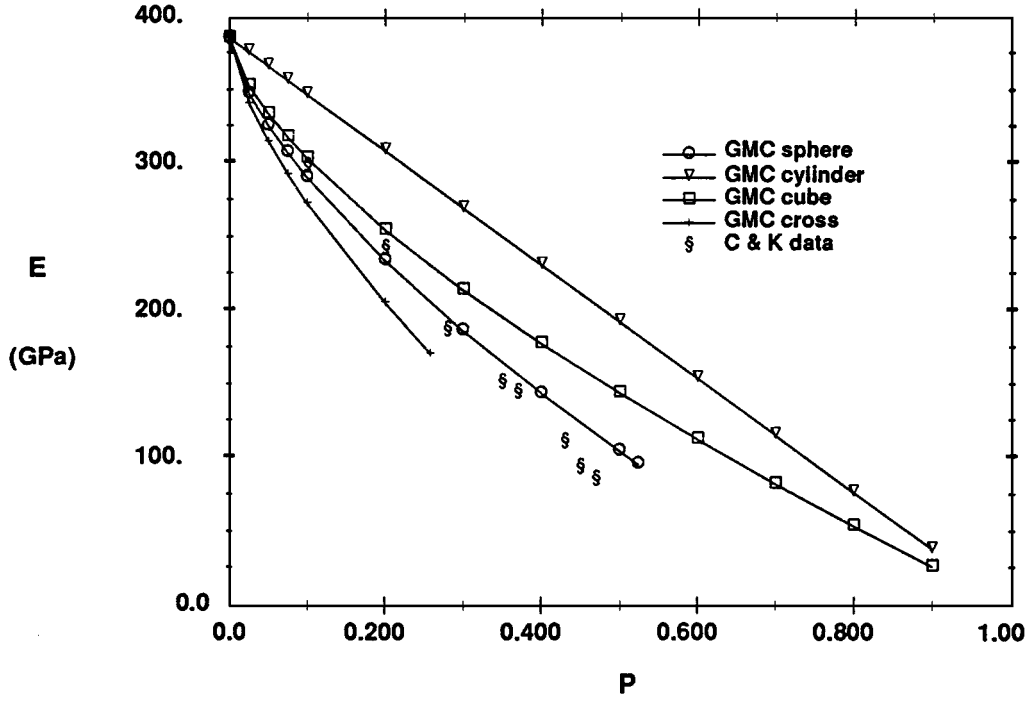

Figure 6 Effective Young's modulus for porous Al_2O_3.

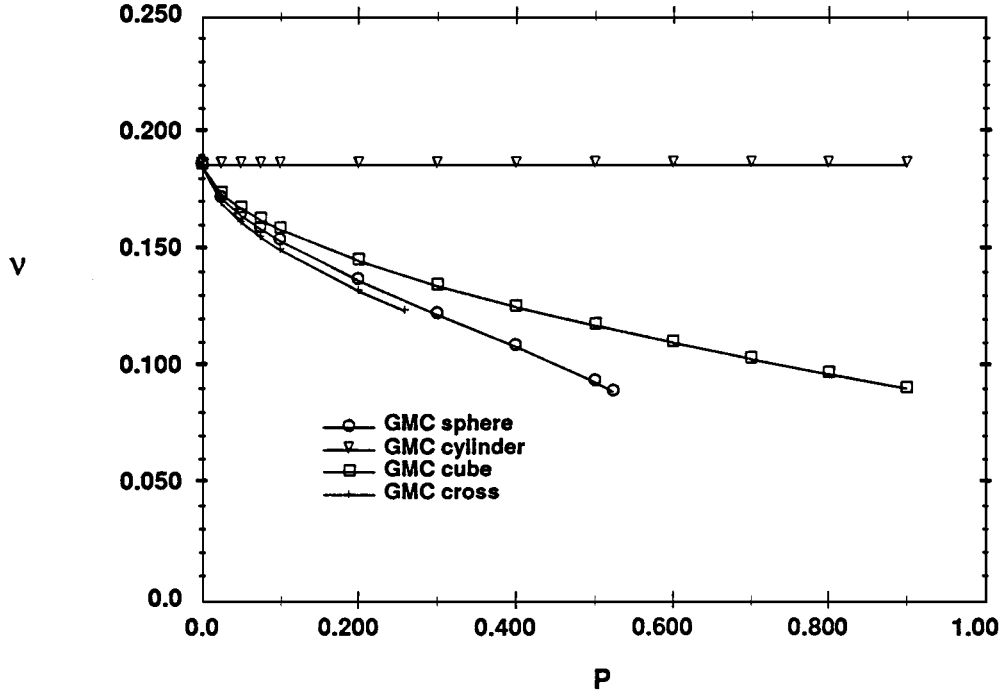

Figure 7 Effective Poisson's ratio for porous Al_2O_3.

100% in some cases) depending upon the pore geometry. It is also evident that whereas the cylindrical pore exhibits a linear dependence on porosity, the dependence is nonlinear for all other pore shapes. The Coble and Kingery experimental results for Young's modulus compare most favorably with the predictions for spherical pores. There is excellent agreement between the spherical pore predictions and experimental values up to a porosity of 0.4. Above $P = 0.4$, the agreement is good but not excellent. This agreement between theory and experiment for spherical pores is consistent with the indication in Ashby and Jones [17] that densification of ceramic powder through sintering results in porosity primarily in the form of small, nearly spherical pores. The shear modulus comparisons in Fig. 8 indicate good correlation with the spherical pore for small P and even better correlation with the cross pore for $0.15 < P > 0.246$.

The independence of Poisson's ratio on porosity for the cylindrical pore geometry (Fig. 7) is a special case in which the effective property is constant and equal to the property of the matrix. This same result can be shown directly from Hill's relations (Hill [18]) for effective elastic properties of two-phase materials with one phase being a void (Benveniste [19]). The predicted decrease in Poisson's ratio as porosity increases for the

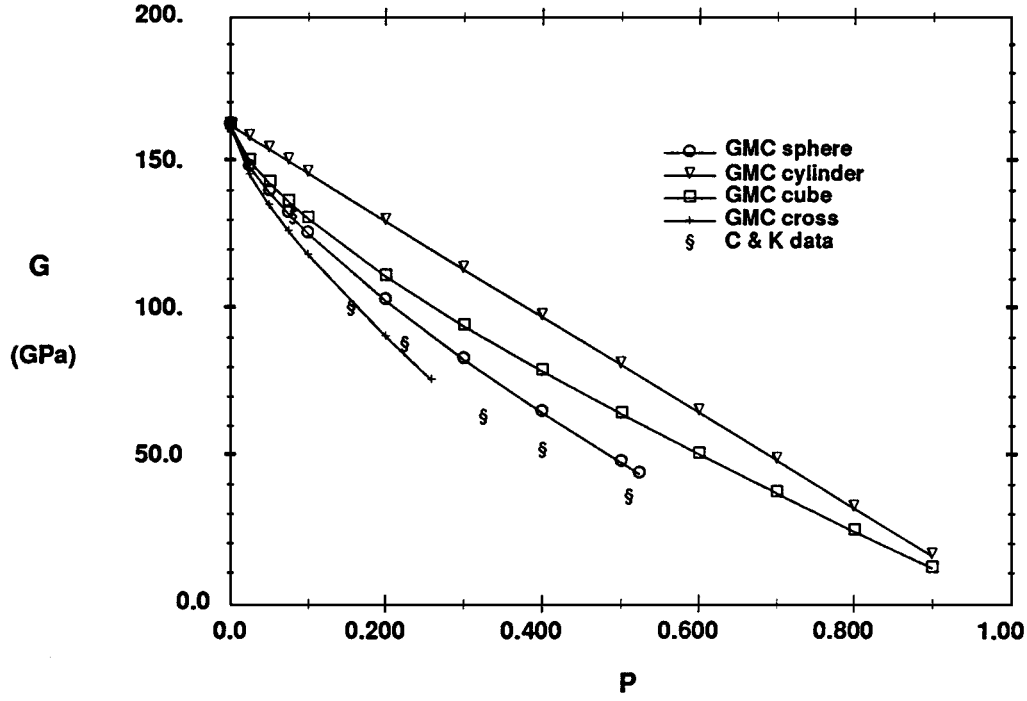

Figure 8 Effective shear modulus for porous Al_2O_3.

other pore shapes is consistent with the experimental results of Coble and Kingery [16]. As mentioned previously, they reported a 50% decrease in Poisson's ratio for $P = 0.5$. Green *et al.* [20] reported only a decrease of approximately 30% for porous alumina at $P = 0.5$. Ashkin *et al.* [21] reported a small increase in Poisson's ratio of porous silica as porosity increased from $P = 0$ to $P = 0.5$ and then a large increase in Poisson's ratio for higher porosity. Their results were based upon measurement of longitudinal and shear wave velocities and the isotropic material property relationship. It would appear that measurement of the dependence of Poisson's ratio on porosity requires direct and accurate measurement of the axial and transverse strains in a tension test. The authors have not found such a set of results in the literature.

Walsh *et al.* [22] obtained experimental results for bulk modulus as a function of porosity by measuring compressibility on a series of glass specimens. Different porosities were produced by varying the sintering temperature for sintered glass powder. The authors reported that microscopic inspection of the specimens after sintering indicated that the pores were primarily spherical, with some pores "slightly ellipsoidal". Young's modulus, E, of the bulk glass was determined to be $E = 10.875 \times 10^6$ psi and Poisson's ratio $\nu = 0.23$. Fig. 9 shows that the GMC predictions (spherical pores) for the bulk modulus as a function of

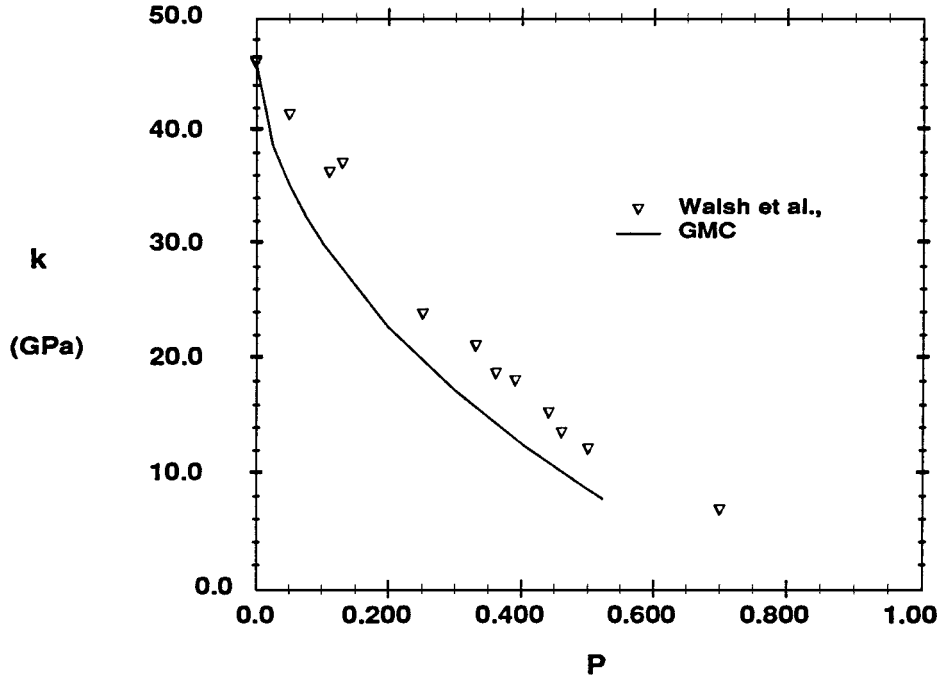

Figure 9 Effective bulk modulus for porous glass.

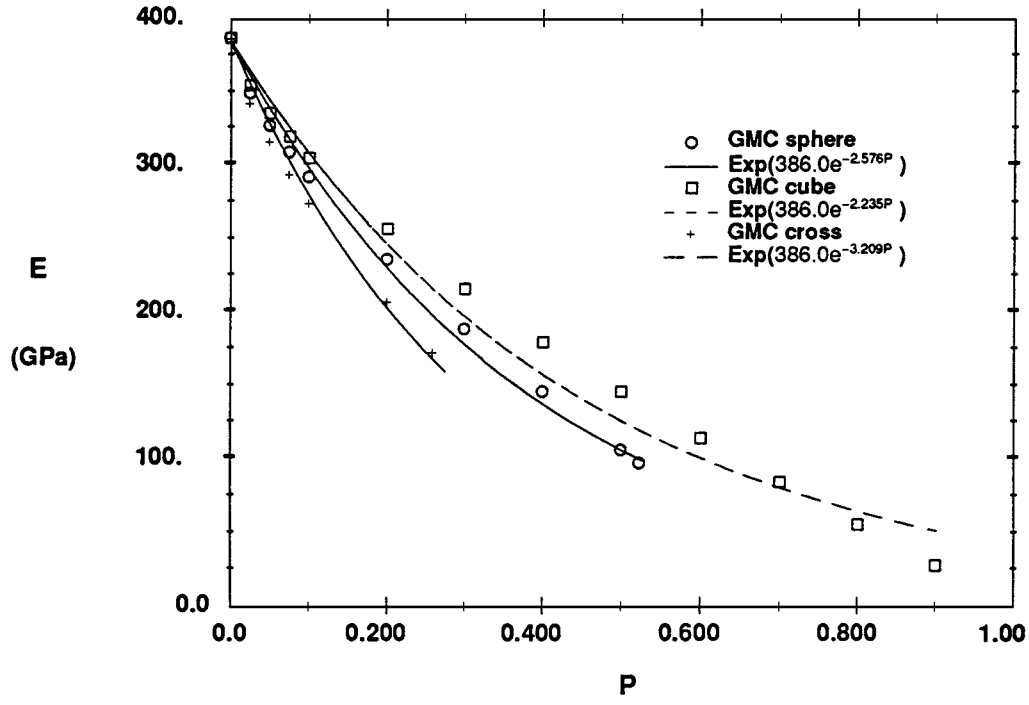

Figure 10 Young's modulus: GMC and exponential.

porosity are slightly lower than the measured values, but generally agree with the experimental results over the range for which predictions are possible. Comparison of the bulk modulus in this case represents a direct comparison of theory and experiment without the need for any assumptions as to the isotropy of the material or the value of other material constants such as Poisson's ratio.

4.2. Comparison with empirical models

4.2.1. Exponential form

Spriggs [23] proposed that the effect of porosity on the effective elastic moduli of ceramic materials could be modeled using an exponential expression of the type suggested by Duckworth [24] and Knudsen [25] as a modification on a form used by Ryshkewitch [26] to describe the effect of porosity on strength. The general form of the equation for an effective modulus M^* of the porous material is an exponential of the form

$$M^* = M_0 \, \mathrm{e}^{-bP} \tag{24}$$

where M_0 is an elastic modulus of the non-porous material, P is the volume fraction of porosity, and b is an empirical constant. This relation has provided a good approximation for effective properties at lower range of porosities, i.e. $P \leq 0.4$ (see Spriggs [23], Spriggs and Brissette [27], and Rice [1]).

After examining experimental data on polycrystalline alumina from several investigators, Spriggs [23] observed that the constant b ranges from 4.08 to 4.35 for hot-pressing; 3.44–3.55 for cold-pressing and sintering; and $b \sim 2.73$ for slip casting and sintering. Since different processing techniques can be associated with different pore structures, this suggests a connection between effective moduli, pore shape and volume fraction, and processing technique.

GMC predictions for the Young's and shear moduli were fit to curves of the exponential form using a modified least squares method to determine the b value corresponding to a best fit for the three included phase pore models. These curves and the b values are shown in Figs 10 and 11. Note that the spherical pore results, $b = 2.576$ for E and $b = 2.405$ for G correspond very well with the value of 2.73 identified by Spriggs for slip casting and sintering, whereas the cross pore values, $b = 3.209$ for E and $b = 2.550$ for G, are more consistent with Spriggs' value for cold-pressing and sintering. Typically, Poisson's ratio has not been described by an exponential relationship. However, if the porous material is assumed isotropic, then the $G = E/2(1+\nu)$ relationship can be used to determine ν.

It is further noted that the results of this curve fitting the GMC results to exponential forms, gives b parameter values that are very similar for E and G. If E and G vary in the same manner with porosity and the porous material is isotropic, then Poisson's ratio is independent of porosity. This is consistent with the results of Ashkin *et al.* [21] discussed previously.

4.2.2. Minimum solid area model

Rice [1, 2] associated the effective properties of porous media with pore shape and packing arrangement by noting that these geometric characteristics are related to the minimum area that transfers load. For one-dimensional loading, this area is the minimum solid area normal to the stress. Under the assumptions of the minimum solid area model, the ratio M^*/M_0, equals the minimum solid area (MSA) for a given pore shape and packing arrangement, i.e.

$$\frac{M^*}{M_0} = MSA \tag{25}$$

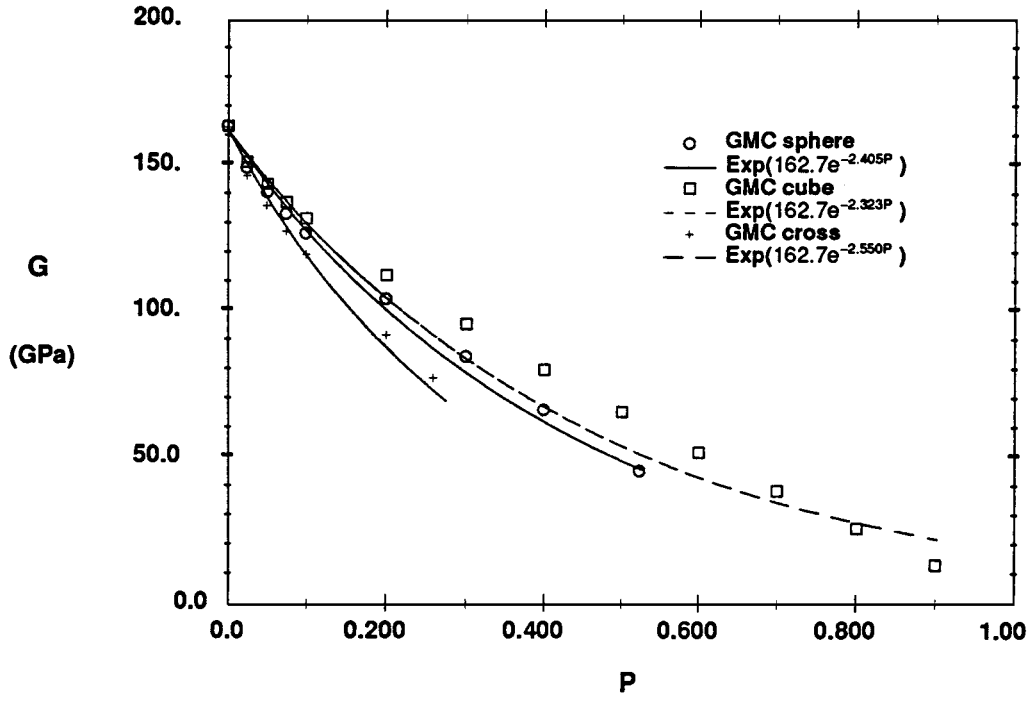

Figure 11 Shear modulus: GMC and exponential.

Because the shapes of the three inclusion pores (cube, cross and sphere) are clearly defined, it is possible to develop exact minimum surface area models for these three pore shapes. Specifically, for loading along a principle axis, the minimum solid area is the cross section of the unit cell less the largest cross section of the pore.

This minimum solid area modeling is applied to the GMC representation of the three inclusion pore shapes as follows:

Cubic pores: The minimum solid area (MSA) for the cubic pore is the area assigned the matrix material in the center cross section of the unit cell. This area is given by

$$MSA_{\text{cube}} = 1 - a^2 \tag{26}$$

and with $a = P^{1/3}$ from (18), this can be written in terms of porosity P as

$$MSA_{\text{cube}} = 1 - P^{2/3} \tag{27}$$

Cross shaped pores: Similarly, the minimum solid area for the cross shaped pore is

$$MSA_{\text{cross}} = 1 - 5a^2 \tag{28}$$

and with $a = (P/7)^{1/3}$ from (20), given in terms of porosity P as

$$MSA_{\text{cross}} \approx 1 - 1.36P^{2/3} \tag{29}$$

Spherical pores: Finally, for the spherical pore

$$MSA_{\text{sph}} \approx 1 - 18.8a^2 \tag{30}$$

which, with $a = (P/65.45)^{1/3}$ from (22) becomes

$$MSA_{\text{sph}} = 1 - 1.15P^{2/3} \tag{31}$$

These equations are similar in form to those discussed by Rice [26]. It is clear from Equations 25, 27, 29 and 31 that the minimum solid area at a fixed porosity is largest for the cubic pore and smallest for the cross shaped pore. Also the rate of change in solid area (decreasing) with respect to increasing porosity is the greatest for the cross shaped pore.

Fig. 12 shows that the GMC predictions for elastic modulus are in excellent agreement with those of Equations 27, 29 and 31 for the three inclusion pore shapes.

Rice [1, 28] demonstrates that Spriggs' exponential model provides a good approximation to the solid area model.

The connection between the minimum solid area model and the exponential form can be established by noting that the first term two terms of a linear expansion of the exponential form can be written as

$$\frac{M^*}{M_0} = \mathrm{e}^{-bP} \approx 1 - bP \tag{32}$$

which is valid for $bP \ll 1$.

Each of the minimum solid area relations (27), (29) and (31) can be rewritten in the same form as (32), i.e.

$$\frac{M^*}{M_0} = 1 - \left(\frac{\alpha}{P^{1/3}}\right)P \tag{33}$$

with $\alpha = 1.0$, 1.15, 1.36 for the three different pore shapes. This suggests that for $\alpha P^{2/3}$ small enough, this can also be written as an exponential, i.e.

$$\frac{M^*}{M_0} \approx \mathrm{e}^{-\beta(P)P} \tag{34}$$

In this case though, the parameter $\beta(P) = \alpha/P^{1/3}$ is not a constant but depends on the porosity. For small changes in porosity this can be further approximated

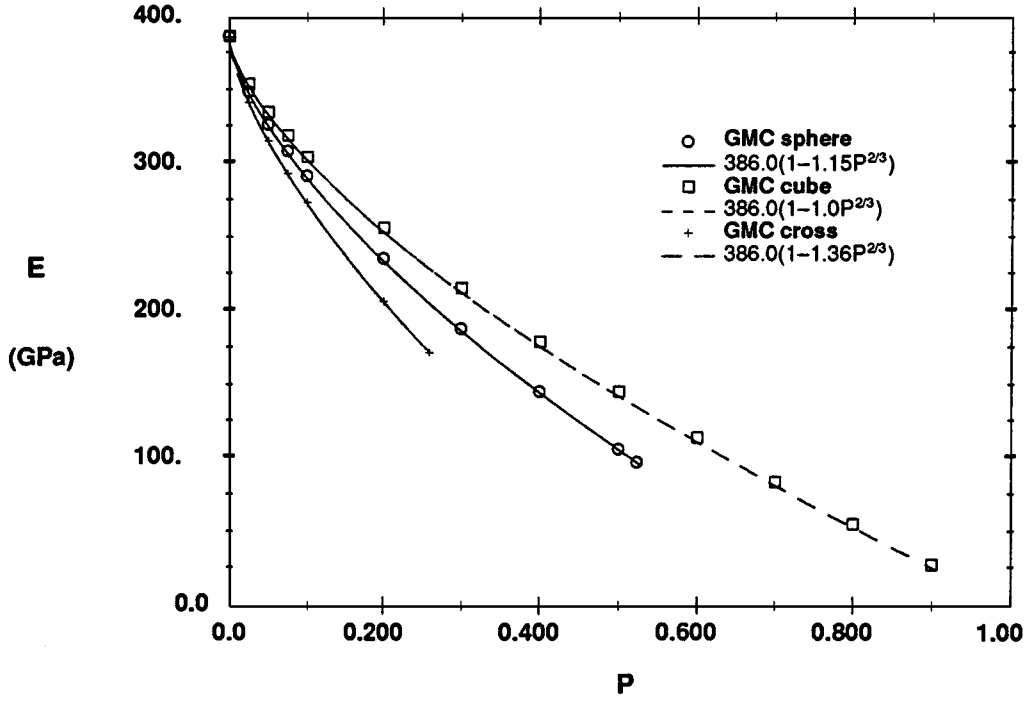

Figure 12 Comparison of minimum solid area model with GMC.

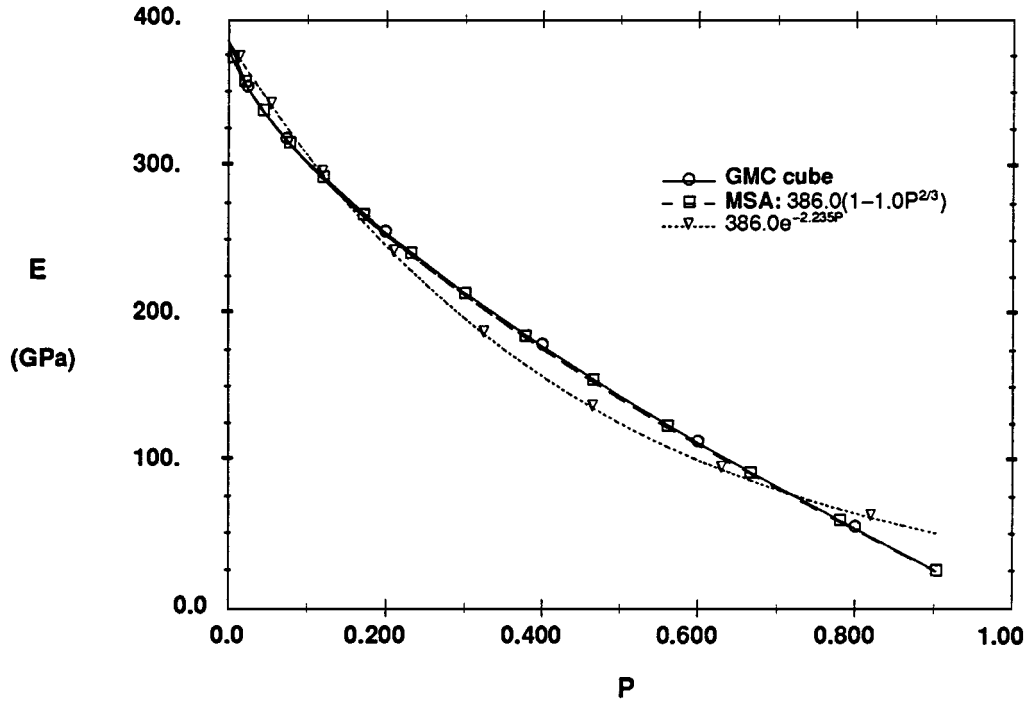

Figure 13 Comparison of GMC, exponential and minimum solid area for cubic pore.

by the exponential form with a constant value of the parameter b.

When comparing pores of different shapes at various porosities, a higher value of b implies that the supporting minimum solid area decreases more rapidly with increasing porosity. General results, predicted by the minimum solid area model and approximated by the exponential form, which are applicable to this work, are that spherical pores in a cubic stacking arrangement will have a $b \sim 3$, (this corresponds to our spherical pore), solid spheres in a cubic stacking arrangement have $b \sim 5$ (this might be a limiting case of the cross pore) and cylindrical pores aligned in the loading direction have $b \sim 1.4$.

Fig. 13 shows that there is excellent correlation between the minimum solid area model and GMC over the full range of porosity. The exponential curve compares reasonably well, however, at higher porosities the exponential curve diverges from the other two models. This is consistent since the exponential approximation is only good for small bP values and was proposed only for porosities below about 0.4.

Rice [2] also examined a wide range of experimental data from the literature with the goal of determining trends that are valid over several sets of data. When possible, he used the b value calculated by the original investigators. In most cases data were obtained graphically and b values were fit visually. For ceramics, Rice

observed the following: (a) the average value of b over all processing techniques is $b \sim 4$; (b) hot pressing, iso-pressing and colloidal pressing give higher b values than cold-pressing. This is attributed to the increased packing densities achieved by the former processing techniques; higher b values are associated with more densely packed materials.

4.3. Comparison with theoretical models

Most of the existing analytic models for the effective properties of porous materials have been developed as a special case of the problem of an inclusion phase in a matrix. A representative element of a two-phase material is analyzed and the results obtained are extended to the continuum material, attempting to take into account the distribution of the included phase and interactions between included phases. Two phase materials are heterogeneous, but if the size, shape and distribution of the included phase are distributed in a statistically random fashion, then it is possible to consider the material as a continuum. Ramakrishnan and Arunachalam [29] summarize the general types of existing theoretical models and cite examples of each method which can be found in the literature.

One such method, referred to as the composite sphere model was developed by Hashin [30]. In this method, a representative sub-volume of a two-phase material is modeled by a sphere of one material surrounded by a spherical sheath of a second material. An assemblage of these layered spheres, of various sizes, is then used to fill the entire space occupied by the continuum material. The specific composition of the material is incorporated into the model by requiring that the relative proportion of the constituent material in each composite sphere remains the same. Hydrostatic pressure is imposed on the assemblage under the assumption that each composite sphere experiences the same pressure. For a two-phase material, Hashin's work provides bounds on the bulk and shear moduli of the composite (see also, Hashin and Shtrikman [31]). When this model is used with a porous medium, i.e., when the included phase is a void, the lower bound collapses to zero and only the upper bound remains. Using this approach, the upper bound on the effective Young's modulus, E^*, is given in terms of the initial modulus, E_0, the initial Poisson's ratio, ν, and the porosity, P, by

$$\frac{E^*}{E_0} \leq \frac{2(7-5\nu)(P-1)}{-14+10\nu-13P+2\nu P+15\nu^2 P} \tag{35}$$

and an upper bound on the shear modulus, G^*, is

$$\frac{G^*}{G_0} \leq \frac{(7-5\nu)(P-1)}{-7+5\nu-8P+10\nu P} \tag{36}$$

where G_0 is the shear modulus of the non-porous material.

Ramakrishnan and Arunachalam [29, 32] adapted a composite sphere modeling approach specifically to model voids as the included phase. They define a non-zero radial stress, which develops at the surface of the composite sphere, and reflects the influence on each pore by its neighbors. Their results for a modulus, M, are of the form

$$\frac{M^*}{M_0} = \frac{(1-P)^2}{(1+\kappa_m P)} \tag{37}$$

where M_0 corresponds to the non-porous property, M^* is the porous property and κ_m is a parameter. For the Young's modulus E, κ_m is

$$\kappa_m \equiv \kappa_E = 2-3\nu \tag{38}$$

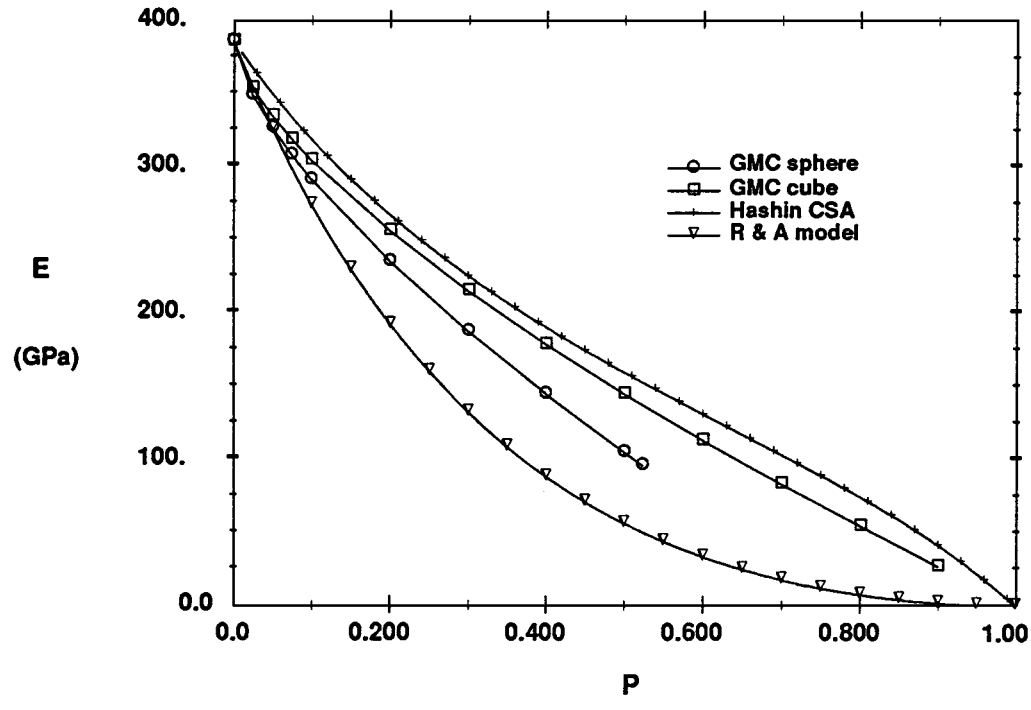

Figure 14 Elastic modulus—composite spheres.

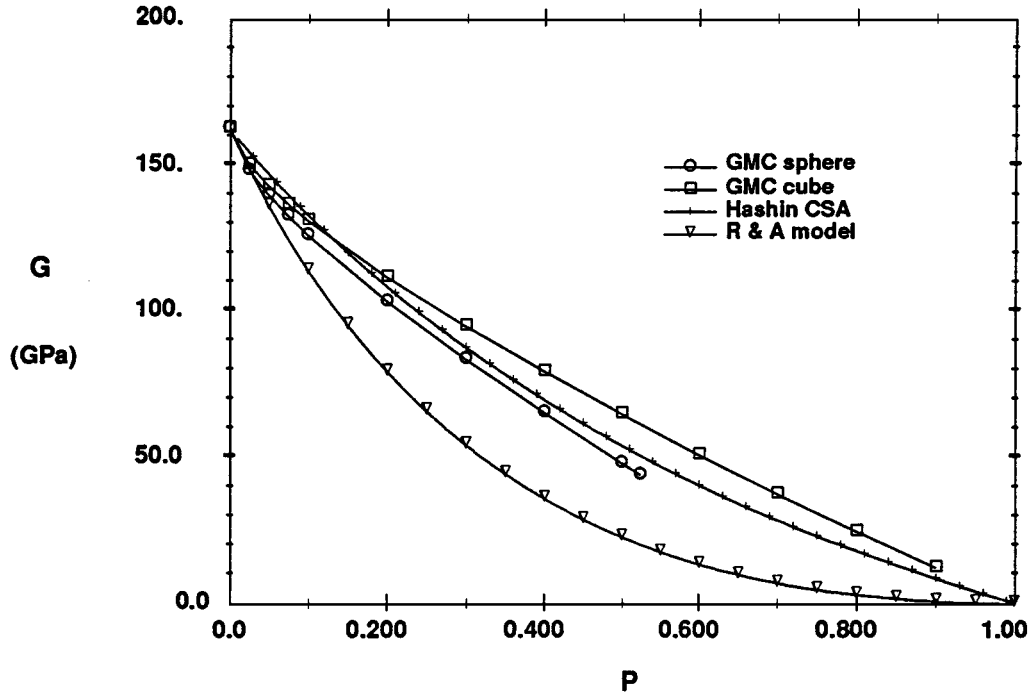

Figure 15 Shear modulus—composite spheres.

and for shear modulus G, κ_m is

$$\kappa_m \equiv \kappa_G = \frac{11 - 19\nu}{4(1+\nu)} \tag{39}$$

Comparisons for Young's modulus and shear modulus, as a function of porosity, as predicted by GMC and the composite spheres models of Hashin [30] and Ramakrishnan and Arunachalam [32] are presented in Figs 14 and 15. The GMC predictions are given for both the cubic and spherical pores. It is evident from the figures that Hashin's composite spheres model, which is an upper bound, agrees most closely with the GMC cubic pore model. Recall that the GMC spherical pore model agrees most closely with the experimental results (see Figs 6 and 8). The Ramakrishnan and Arunachalam model predicts values considerably below the other predictions and the experimental values.

4.4. Theoretical-experimental comparisons

Comparisons between the Coble and Kingery experimental data for the Young's modulus of porous alumina with the predictions of GMC, the minimum solid area model and the exponential model for cubic, cross, and spherical pores are presented in Figs 16 to 18. As noted

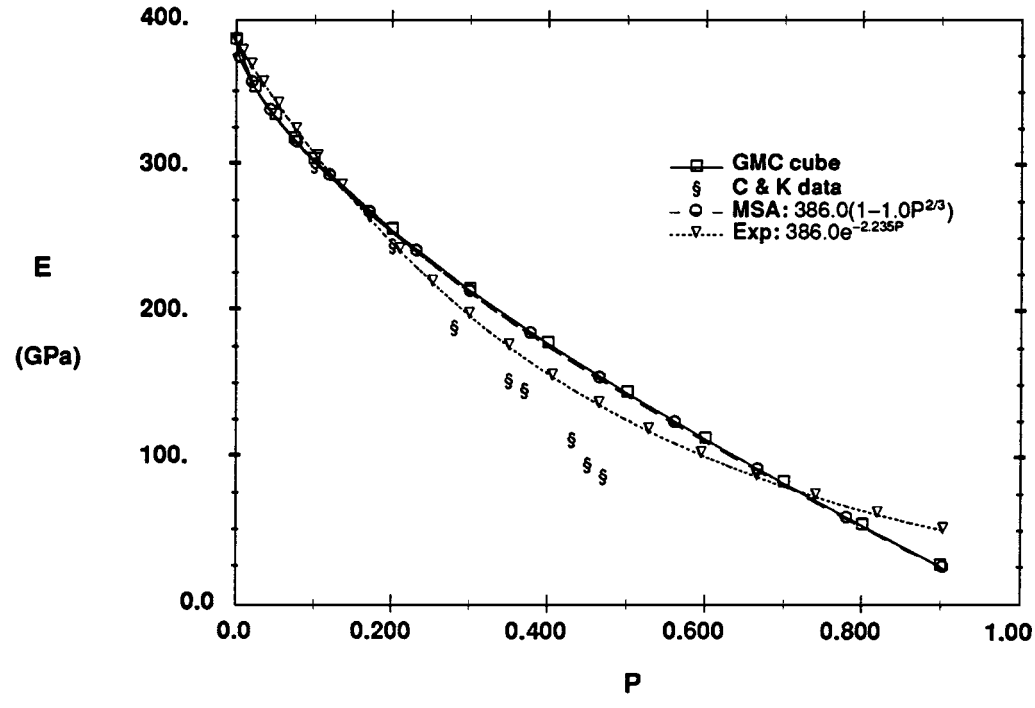

Figure 16 Modulus comparisons for cubic pores.

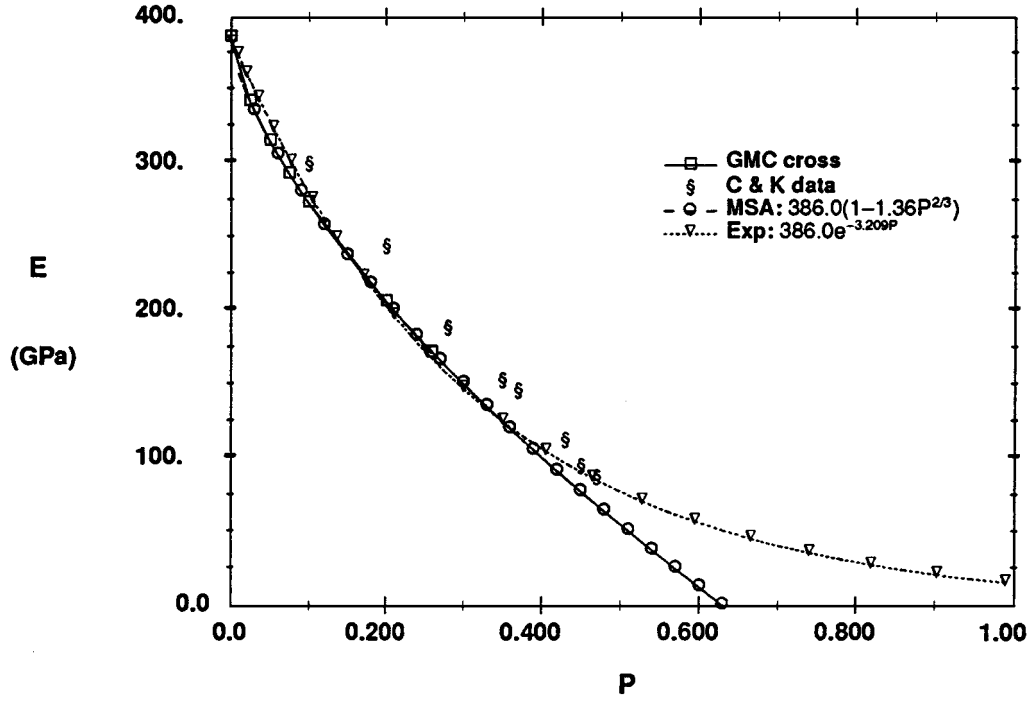

Figure 17 Modulus comparisons for cross pores.

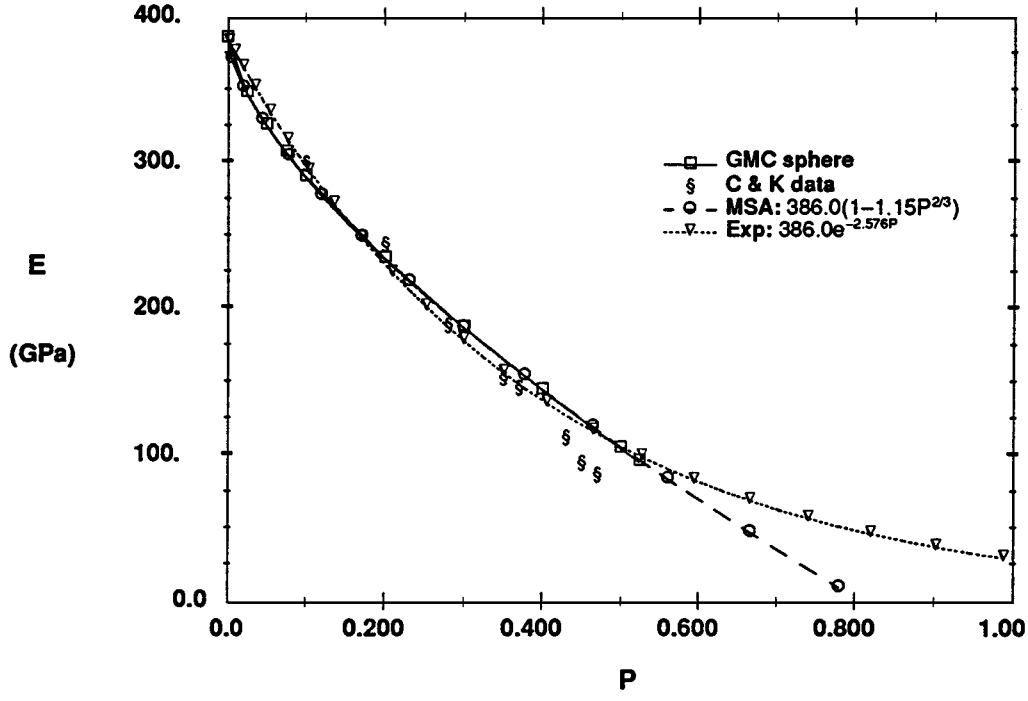

Figure 18 Modulus comparisons for spherical pores.

previously, the spherical pore provides the best correlation between theory and experiment with the cross pore being the next best. In all cases, the GMC and minimum solid area predictions are essentially identical.

4.5. Nonlinear response

GMC has the added capability of predicting the nonlinear response of porous media. Figs 19 and 20 show predictions for the nonlinear tensile response of the intermetallic nickel compound IC-50 as a function of pore geometry at a porosity of 0.2 (Fig. 19), and as a function of porosity for spherical pores with P ranging from 0.025 to 0.4 (Fig. 20). The Bodner-Partom parameters (see [13]) used to model the visco-plastic response of the IC-50 are: $E = 180$ GPa, $\nu = 0.3$, $G = 69.24$ GPa, $Z_0 = 370$ MPa, $Z_1 = 640$ MPa, $m = 150$, $n = 22$ and $q = 1$.

As indicated in Fig. 19, the results indicate that the yield stress is a strong function of the pore geometry with the cross pore exhibiting the lowest yield stress and the cylindrical pore exhibiting the highest yield stress. For this specific case of $P = 0.2$, the yield stress varies by as much as 50% with change in pore geometry. As indicated in Fig. 20, the porosity has an even stronger influence on the yield stress. The yield stress varies by

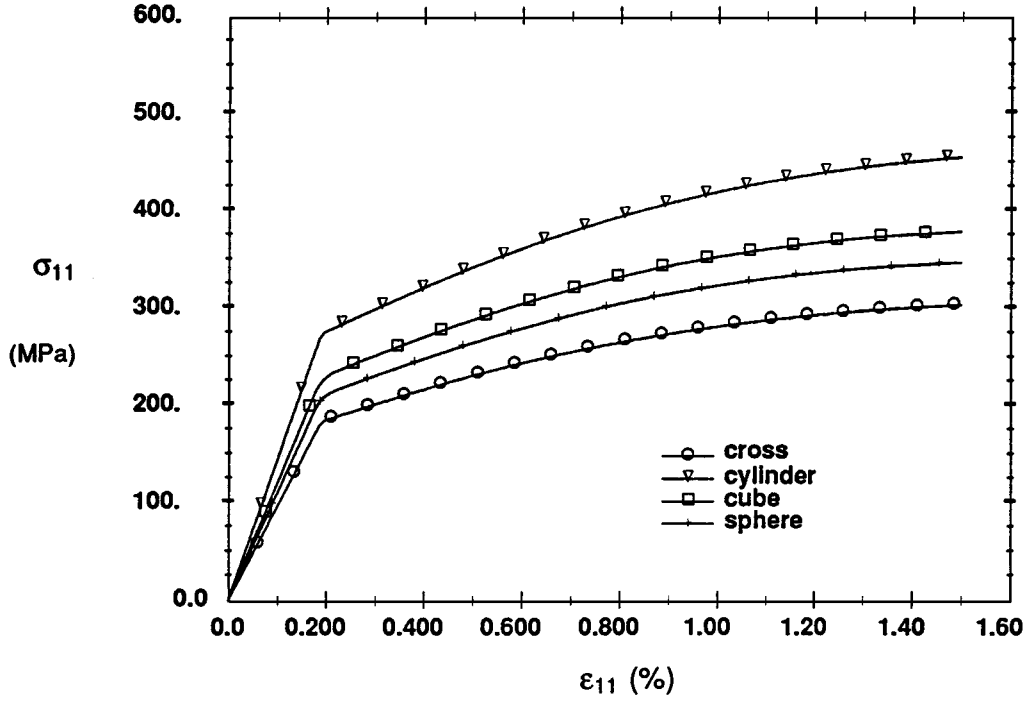

Figure 19 Nonlinear response—pore geometry dependence.

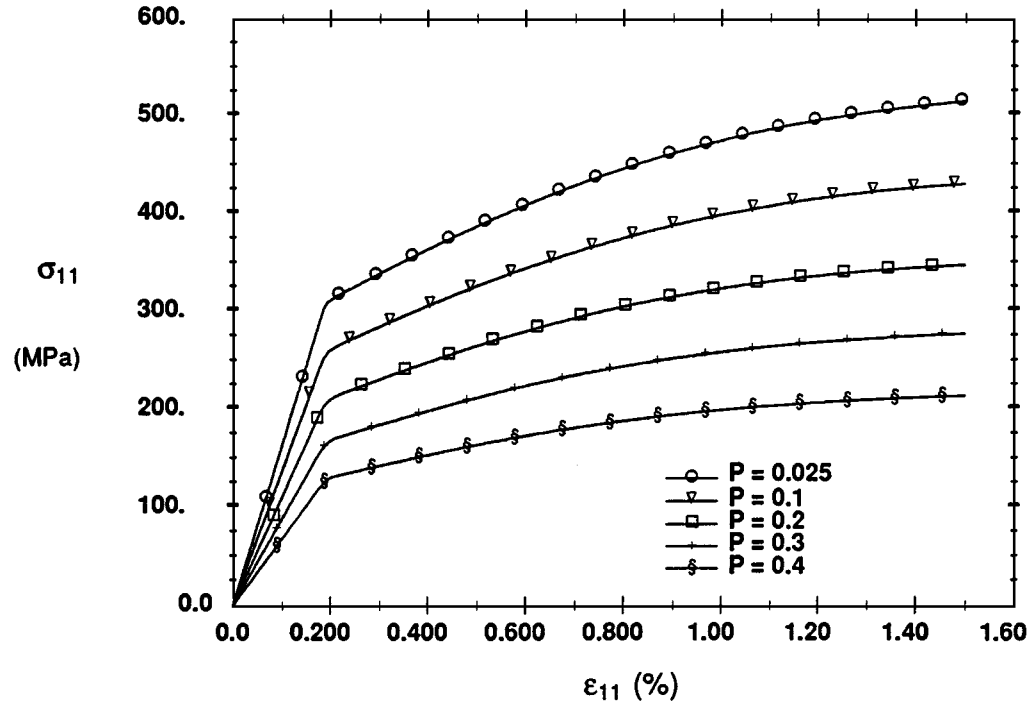

Figure 20 Nonlinear response—porosity dependence.

as much as a factor of three for spherical pores as the porosity ranges from $P = 0.025$ to $P = 0.4$. Close examination of the results also indicates that there is much stronger strain hardening behavior for small porosity. As the porosity increases, the strain-hardening behavior approaches the perfectly-plastic case.

5. Conclusions

It has been shown that the generalized method of cells can be used to study the influence of pore geometry on the elastic and inelastic response of porous media. Periodic microstructures with four distinct pore geometries were studied and the results for effective elastic properties were compared with several other available models and some experimental results. Predictions for the inelastic response of porous media were presented for tensile loading, as a function of pore geometry and pore volume fraction, with the inelastic behavior of the bulk material modeled using a unified visco-plasticity theory. All results were presented for discrete pore shape and discrete porosity. It was shown that pore geometry can have a significant influence on both elastic and inelastic response, that pore geometry can be associated with parameters of other available models, and that the generalized method of cells is an

efficient, flexible and reliable method of analysis for such problems. GMC modeling has provided a correlation between pore geometry and the b parameter of exponential models for effective elastic properties. It has also been shown that GMC, the exponential model and the minimum solid area models are in good agreement for a given pore geometry. Comparison of the predictions with experimental results for aluminum oxide and a sintered glass indicates that modeling the porosity as spherical pores or cross pores provides good correlation between theory and experiment. Finally, it has been shown that GMC can be used to model the inelastic response of porous media as a function of pore geometry and pore volume fraction and that the yield stress of the porous medium is a strong function of both characteristics, whereas the strain-hardening response is only a strong function of the porosity.

Acknowledgement

This work was supported by the Air Force Office of Scientific Research through AFOSR Grant No. F49620-93-1-0359. Dr. Walter F. Jones and Captain Brian Sanders serve as the technical monitors. This support is gratefully acknowledged as are the most helpful comments of Professor Aboudi.

References

1. R. W. RICE, *J. Mater. Sci.* **31** (1996) 102.
2. *Idem., ibid.* **31** (1996) 1509.
3. L. J. GIBSON and M. F. ASHBY, "Cellular Solids, Structure & Properties" (Pergamon Press, Oxford, 1988).
4. B. BUDIANSKY, *J. Mech. Phys. Solids* **13** (1965) 233.
5. J. K. MACKENZIE, *Proc. Phys. Soc.* **62** (1950) 2.
6. S. NEMAT-NASSER and M. TAYA, *Quart. Appl. Math.* **39** (1981) 43.
7. T. Y. CHU and Z. HASHIN, *Int. J. Eng. Sci.* **9** (1971) 971.
8. M. M. CARROLL and A. C. HOLT, *J. Appl. Phy.* **43** (1972) 1626.
9. B. M. BUTCHER, M. M. CARROLL and A. C. HOLT, *ibid.* **45** (1974) 3864.
10. J. ABOUDI, *Mechanics of Materials* **3** (1984) 81.
11. PALEY and ABOUDI, *ibid.* **14** (1992) 127.
12. J. ABOUDI, in "Damage in Composite Materials," Vol. 3, edited by G. Z. Voyiadjis (Elsevier Science 1993).
13. S. R. BODNER and Y. PARTOM, *J. Appl. Mech.* **42** (1975) 385.
14. J. ABOUDI, *Int. J. Eng. Sci.* **20**(5) (1982) 605.
15. Z. QIAN, J. M. DUVA and H. N. G. WADLEY, *Acta Mater.* **44**(12) (1996) 4815.
16. R. L. COBLE and W. D. KINGERY, *J. Amer. Ceram. Soc.* **39**(11) (1956) 377.
17. M. F. ASHBY and D. R. H. JONES, "Engineering Materials 2, an Introduction to Microstructures, Processing and Design" (Pergamon Press, Oxford, 1986) p. 179.
18. R. HILL, *J. Mechanics and Physics of Solids* **12** (1964) 199.
19. Y. BENVENISTE, Tel Aviv University, private communication (1996).
20. D. J. GREEN, C. NADER and R. BREZNY, *Ceram. Trans.* **7** (1990) 345.
21. D. ASHKIN, R. A. HABER and J. B. WACHTMAN, *J. Amer. Ceram. Soc.* **73**(11) (1990) 3376.
22. J. B. WALSH, W. F. BRACE and A. W. ENGLAND, *ibid.* **48**(12) (1965) 605.
23. R. M. SPRIGGS, *ibid.* **44**(12) (1961) 628.
24. W. DUCKWORTH, *ibid.* **36**(2) (1953) 68.
25. F. P. KNUDSEN, *ibid.* **42** (1959) 376.
26. RYSHKEWITCH, *ibid.* **36**(2) (1953) 65.
27. R. M. SPRIGGS and L. A. BRISSETTE, *ibid.* **45**(4) (1962) 198.
28. R. W. RICE, *J. Mater. Sci.* **28** (1993) 2187.
29. A. RAMAKRISHNAN and V. S. ARUNACHALAM, *J. Amer. Ceram. Soc.* **76**(11) (1993) 2745.
30. Z. HASHIN, *J. Appl. Mech.* **29**(1) (1962) 143.
31. Z. HASHIN and S. SHTRIKMAN, *J. Mech. Phys. Solids* **11** (1963) 127.
32. A. RAMAKRISHNAN and V. S. ARUNACHALAM, *J. Mater. Sci.* **25** (1990) 3930.

Received 8 August 1997
and accepted 26 October 1998